Journal of
Materials Chemistry B

Materials for biology and medicine

Accepted Manuscript

This article can be cited before page numbers have been issued, to do this please use: P. Naserzadeh, M. Namvari, A. Razmi and S. Agah, *J. Mater. Chem. B*, 2026, DOI: 10.1039/D6TB00505E.

This is an Accepted Manuscript, which has been through the Royal Society of Chemistry peer review process and has been accepted for publication.

Accepted Manuscripts are published online shortly after acceptance, before technical editing, formatting and proof reading. Using this free service, authors can make their results available to the community, in citable form, before we publish the edited article. We will replace this Accepted Manuscript with the edited and formatted Advance Article as soon as it is available.

You can find more information about Accepted Manuscripts in the Information for Authors.

Please note that technical editing may introduce minor changes to the text and/or graphics, which may alter content. The journal's standard Terms & Conditions and the Ethical guidelines still apply. In no event shall the Royal Society of Chemistry be held responsible for any errors or omissions in this Accepted Manuscript or any consequences arising from the use of any information it contains.

ROYAL SOCIETY OF CHEMISTRY

rsc.li/materials-b

View Article Online
DOI: 10.1039/D6TB00505E

MXene-Based Protective Strategy for Diabetic Gingival Wound Healing: Shielding Fibroblasts from Oxidative Stress

Parvaneh Naserzadeh[1*], Mina Namvari[2*], Abbas Razmi[3], Shahram Agah[1]

[1]Colorectal Research Center, Iran University of Medical Sciences, Tehran, Iran

[2]Sabanci University Nanotechnology Research and Application Centre (SUNUM), Tuzla, Istanbul, Türkiye

[3]Faculty of Engineering, Department of Mechanical Engineering, Ataturk University, Erzurum, Türkiye

Corresponding authors: Dr. Parvaneh Naserzadeh, Email: naserzadeh.p@iums.ac.ir

Dr. Mina Namvari, Email: mina.namvari@sabanciuniv.edu

Parvaneh Naserzadeh ORCID ID https://orcid.org/0000-0001-6763-687X

Mina Namvari ORCID ID https://orcid.org/0000-0003-2457-1484

Abbas Razmi ORCID ID https://orcid.org/0000-0002-5012-6694

Shahram Agah ORCID ID https://orcid.org/ 0000-0002-5269-4644

View Article Online
DOI: 10.1039/D6TB00505E

Abstract

The bidirectional association between diabetes mellitus (DM) and periodontitis remains a major focus in oral and systemic health research. DM is a key risk factor influencing the onset, progression, and severity of periodontitis, yet the molecular mechanisms underlying this relationship are not fully understood. Periodontitis is characterized by bacterial biofilm formation and a destructive host immune-inflammatory response. In this study, we explored the therapeutic potential of $Ti_3C_2T_x$ MXene, a two-dimensional nanomaterial, for enhancing gingival wound healing in diabetic conditions. $Ti_3C_2T_x$ MXene treatment of fibroblast cells derived from diabetic rat gingival tissue modulated oxidative stress and restored glutathione balance. The material exhibited significant biocompatibility, preserved mitochondrial membrane potential, and reduced intracellular reactive oxygen species (ROS) levels. Moreover, $Ti_3C_2T_x$ MXene influenced lipid peroxidation and cytochrome c release, contributing to controlled caspase activation and balanced apoptotic responses. These results suggest that $Ti_3C_2T_x$ MXene supports cellular and mitochondrial homeostasis, promoting improved wound repair in diabetic gingiva. Collectively, this study presents the first evidence of $Ti_3C_2T_x$ MXene as a promising nanotherapeutic platform for managing diabetic oral wounds and potentially other chronic wounds, paving the way for future applications in nano-enabled topical formulations and interdisciplinary oral healthcare strategies.

Keywords: $Ti_3C_2T_x$ MXene, Periodontitis, Diabetes, Gingival Wound Healing, Oxidative Stress.

Introduction

Diabetes mellitus (DM) is a metabolic disorder marked by persistently high blood glucose levels. It is recognized as one of the major causes of both macrovascular and microvascular complications.[1, 2] Individuals with diabetes tend to experience a higher incidence and faster progression of periodontal disease, largely due to their increased vulnerability to infections.[3] Periodontal disease involves inflammation of the gums triggered by pathogenic bacteria, which results in gradual destruction of the alveolar bone surrounding affected teeth. Growing evidence supports a two-way relationship between DM and periodontal disease.[4-6] In diabetic patients, dental healing is often compromised. This impaired repair process involves reduced neutrophil function, limited fibroblast migration and proliferation, and hindered angiogenesis under diabetic conditions.[7, 8] Consequently, diabetic individuals generally respond less favorably to periodontal therapy.[9, 10] Elevated levels of advanced glycation end products (AGEs) are found in the gingival tissues of

View Article Online
DOI: 10.1039/D6TB00505E

diabetic patients[11] contributing to oxidative stress and promoting more rapid tissue damage. These AGEs disrupt normal cell–matrix interactions by modifying extracellular matrix cross-linking, further delaying wound healing.[12] Traditionally, wound management has relied on medications combined with natural or synthetic materials that maintain a warm, moist environment to support healing and minimize microbial infection. Despite their widespread use, these conventional approaches often show limited efficacy because therapeutic agents can be absorbed systemically, diminishing their targeted action at the wound site.[13] To overcome these limitations, researchers have investigated new materials and technologies for diabetic wound repair, including growth factors,[14] engineered grafts,[15, 16] hydrofibers,[17] synthetic polymers,[18] hydrocolloid dressings,[19] and silver-based dressings.[20] Yet, these advanced therapies also face several obstacles—such as delayed epithelialization, allergic responses, irregular bioactive compound release, cytotoxicity, impaired angiogenesis, physiological rejection, and degradation of growth factors at diabetic ulcer sites.[13] More recently, attention has shifted toward nanotechnology-driven solutions in clinical practice, primarily due to the unique characteristics of nanomaterials.[21] With particle sizes typically between 1 and 100 nm, they possess a high surface-area-to-volume ratio and exhibit distinctive optical, electrical, and thermal properties.[22-25] These nanoscale materials hold promise for improving treatment efficacy and reducing adverse effects in chronic diabetic wound care.[26]

MXenes are a novel class of two-dimensional (2D) nanomaterials composed of transition metal carbides, nitrides, or carbonitrides. They follow the general formula $M_{n+1}X\square T_x$ (n = 1–3), where M represents an early transition metal such as titanium (Ti), niobium (Nb), or molybdenum (Mo); X denotes carbon and/or nitrogen; and T_x corresponds to surface terminations like –O, –F, –Cl, or –OH.[27, 28] Since its discovery,[29] MXenes have garnered increasing attention owing to their graphene-like features and superior physicochemical properties, including large specific surface area, high electrical conductivity, remarkable mechanical strength, , hydrophilicity, and efficient photothermal conversion.[30, 31] Owing to their unique properties, MXenes have emerged as promising candidates for energy conversion and storage, catalysis, antimicrobial membranes, and a wide range of biomedical applications.[24, 28, 32-34]

To date, only a few types of MXenes have been explored for biological and biomedical applications,[35] such as Ti_2CT_x,[36] $Ti_3C_2T_x$,[37] and Nb_2CT_x.[38] Among these, $Ti_3C_2T_x$ has been the most extensively investigated, primarily due to its relatively straightforward synthesis process. A notable attribute of MXenes is their strong near-infrared absorption, which shows promise in theranostic platforms and photothermal therapies, including combination cancer treatments.[39-44]

View Article Online
DOI: 10.1039/D6TB00505E

Their hydrophilic nature and rich surface functionalities, provide versatile sites for binding biologically active molecules, making them excellent candidates for biomedical interfacing.[45] However, a key concern surrounding the application of MXenes in biological systems is their potential cytotoxicity. Cytotoxicity refers to the capacity of a substance to damage or kill cells, typically through mechanisms involving oxidative stress, excessive generation of reactive oxygen species (ROS), and subsequent cellular apoptosis or necrosis.[46] While some toxicity stems from intrinsic biological variations such as genetic and metabolic differences, extrinsic factors related to the nanomaterial itself including chemical composition, solubility, size, surface chemistry, morphology, and aggregation play a significant role. Toxic substances may compromise cell membrane integrity, reduce cell viability, and hinder cellular proliferation.[47] Current evidence indicates that the cytotoxicity and biocompatibility of MXenes are highly dependent on multiple physicochemical and experimental factors, including synthesis method, oxidation state, surface functionalization, layer structure (single- versus multilayered), particle size, concentration, exposure duration, and route of administration. Both in vitro and in vivo studies consistently show that variations in these parameters determine whether MXenes elicit toxic or biocompatible responses.[46, 48-51] Notably, pristine single-layer $Ti_3C_2T_x$ nanosheets exhibit high compatibility with a variety of cell types and have shown promise as scaffolds for tissue culture applications.[48]

Despite the growing scientific interest in MXenes for a wide range of technological applications, studies assessing their cytotoxicity remain relatively scarce. A MXene-based composite has been reported to detect hydrogen peroxide for the indication of periodontal disease [52] and an injectable MXene-loaded hydrogel was investigated in management of inflammation control and bone regeneration in severe periodontitis,[53] however, to the best of our knowledge, there is no investigation of the effect of MXene in diabetic gingival wound healing. In the present study, we prepared $Ti_3C_2T_x$ MXene-based nanodrug formulations and investigated their therapeutic potential in promoting the healing of diabetic gingival wound by regulating oxidative stress pathways and boosting glutathione activity in fibroblast cells isolated from diabetic rat models.

2. Materials and Methods

2.1. Chemicals and Materials

Ti_3AlC_2 (325 Mesh, Purity: 99+%) was purchased from Nanografi (Ankara, Turkey). Lithium fluoride (LiF) and concentrated HCl were obtained from ThermoFisher Scientific and Merck, respectively. 3-[4,5-dimethylthiazol-2-yl]-2,5-diphenyltetrazolium bromide (MTT), dimethyl

View Article Online
DOI: 10.1039/D6TB00505E

sulfide (DMSO), 2′,7′-dichlorofluorescein diacetate (DCFH-DA) probes, malondialdehyde (MDA), thiobarbituric acid (TBA), N-butanol, tetramethoxypropane (TEP), O-phthalaldehyde, (OPA) probe, N-ethylmaleimide (NEM) probe were purchased from Sigma-Aldrich. Mouse/Rat Cytochrome C ELISA Kit (AB210575) was purchased from Abcam. Annexin V-FITC/PI Apoptosis Kit (E-CK-A211) and Acridine Orange (A1301) were purchased from Elabscience and Invitrogen, respectively, blood glucose meter (GLUCOCARD G Black, ARKRAY, Inc.)

2.2. Instruments

Incubator 37 °C, Sensor CO_2 Sanyo, Japan MCO; Refrigerated Centrifugation, Sanyo, Harrier 18/80, Japan; Floremetry, Shimadzu RF-5000, Japan; Digital scale Japan; Shaker, REAX2000, Iran; ELISA reader, Infinite 200 PRO, Tecan, Basel Switzerland; Flowcytometry, BD Biosciences FACS Calibure TM flow cytometer, USA. The structure MAX phase and MXene were analyzed using an X-ray diffractometer (XRD) (Bruker D2 advance, Germany) with monochromatized Cu-Kα radiation (λ = 1.54184 Å) generated at 30 kV and 10 mA, with a scan rate of 1°/min and a step size of 0.05°. The morphological structure of the materials was visualized by JSM-6010LA. X-ray photoelectron spectroscopy (XPS, the Thermo Scientific KAlpha) was used to analyze the compositions of the samples. The hydrodynamic diameters and zeta potential of aqueous samples in ultrapure water were determined at 25 °C using a Zetasizer Pro (Model MAL1256845, Malvern Panalytical Ltd., UK). Each test was repeated three times, and an averaged value was derived to ensure accuracy.

2.3. Synthesis of $Ti_3C_2T_x$ MXene

$Ti_3C_2T_x$ MXenes was synthesized according to previous literature.[32, 37] 2 g of LiF was mixed with 40 ml of 6 M HCl and stirred for 10 minutes. Subsequently, 2 g of Ti_3AlC_2 powder was gradually introduced into the mixture and agitated at a temperature of 40 ºC for 45 hours. Following the etching procedure, the sediments obtained were rinsed several times using deionized water and subjected to centrifugation at a speed of 3500 rpm for 5 minutes, until the pH approached nearly 6. Additional water was introduced to the sediment, which was then bath sonicated for 30 minutes under N_2 gas and centrifuged at a speed of 10000 rpm for 30 minutes to collect the supernatant as few-layer MXene. The final product was obtained by freeze-drying after 3 days.

View Article Online
DOI: 10.1039/D6TB00505E

2.4. Experimental design

2.4.1. Preparation of animals

We acquired Sprague-Dawley male rats (total number =20, 5 animals per group) from Tehran Medical University in Tehran, Iran. The sample size was established based on a priori power analysis, utilizing an expected effect size derived from preliminary studies. This analysis indicated adequate power (≥80%) to identify statistically significant differences (α=0.05) in the primary outcomes related to cell population metrics. This methodology ensures the collection of reliable data while strictly adhering to the 3Rs principle, which emphasizes the reduction of animal use in research. Furthermore, the subsequent cellular analyses involved the quantification of over 10,000 individual cells from these biological replicates, thereby increasing the statistical confidence in the resulting population data. These rats were all the same age, measuring around 8-10 weeks, and weighing approximately 150 g. They were housed in controlled conditions, including a temperature range of 20-12 °C, humidity levels between 50-60%, and a consistent 12-hour cycle of light and dark. Furthermore, the rats had unrestricted access to tap water and were given standard food.

Animals were divided into 4 groups which were treated as following: Group 1: Control group received only sterile phosphate-buffered saline (PBS) and served as the healthy control groups (CH). Group 2: Diabetic group received PBS and served as the disease control groups (CD). Group 3: Diabetic group and gingival wound (CDD). Group 4: Diabetic group with gingival wound that received $Ti_3C_2T_x$ MXene (CDDM). All experiments were approved by research ethic committee of Iran University of Medical Sciences with IR.IUMS.AEC.1403.009 Ethical code.

2.4.2. Preparation of animal models and surgical procedure

The animals were injected with streptozotocin (STZ) at a dose of 65 mg/kg of body weight via intravenous administration. STZ induces diabetes within three days by destroying the beta cells. Diabetic and non-diabetic control groups were housed individually in metabolic cages, where their feeding and metabolism were monitored, and blood glucose levels were measured using a commercial glucometer. Rats with blood glucose levels exceeding 10 mmol/L were classified as diabetic. Prior to anesthetic induction, the rats were fasted for 4 to 6 hours, while maintaining ad libitum access to water. Anesthesia was initiated by placing the animals in an induction chamber with 3.0–4.0% isoflurane vapor delivered in oxygen until all motor reflexes were abolished. For

View Article Online
DOI: 10.1039/D6TB00505E

maintenance, the animals were transferred to a heated surgical surface set at 37˚C and were ventilated via a nose cone delivering 1.2–2.0% isoflurane.[54] Blood was collected from the tail vein of each animal without anesthesia between 9:00 and 10:00 AM using heparin-coated or EDTA-coated microhematocrit capillaries at baseline and on days 0, 7, 14, 21, and 28. Blood glucose levels were measured using a glucometer. The HA-8180T device assesses HbA1c levels using reversed-phase distribution exchange chromatography. A blood sample, diluted with a hemolysis and washing solution, is loaded onto the column, where it is fractionated and eluted into each Hb component using HPLC. The eluted components are quantified with an ELISA reader operating at wavelengths of 420 nm and 500 nm.[55]

Operations were performed under sterile conditions. Rats were anesthetized by intracardiac injection of sodium pentobarbital. Anesthesia was maintained by inhalation of halothane (1.5-2.0 vol %). The root of the nose was shaved and disinfected using 70% ethanol. Local anesthesia was implemented using 2% xylocaine/epinephrine. A mucosal flap was made to expose the gum laterally. Dental holes were made at the eye level and 7 mm lateral toward the midline into the gum area, using a 1-mm diameter, 4-mm long slow-speed dental drill under sterile saline irrigation. The $Ti_3C_2T_x$ MXene was inserted into the hole using a sterile spatula. Tetracycline hydrochloride paste was injected into the surgical site to prevent bacterial infection.[56]

2.4.3. Preparation of $Ti_3C_2T_x$ MXene suspension for topical application

The dose per application was calculated based on the wound surface area and a target dose range of 330 µg/mL. This dose range was selected to achieve a local effective concentration (the IC50 of $Ti_3C_2T_x$ MXene was 34.83 µg/mL, aiming for 175–350 µg/mL in non-surgical tissue, after 72h) while accounting for the small wound size and the potential for rapid clearance. A volume of 3 µL of the respective $Ti_3C_2T_x$ MXene was carefully applied directly onto the wound surface using a micropipette.

2.5. Isolation of skin fibroblast cells

The tissue was extracted and washed in PBS and left for 10 minutes in an incubator at 37 °C with 5% CO_2 and 85% humidity, to enhance their adhesion to the plastic surface. DMEM culture medium was then carefully added. Tissue cultures were incubated at 37°C in a humidified incubator with 5% CO_2 until confluent fibroblast layers were obtained.[57]

View Article Online
DOI: 10.1039/D6TB00505E

2.6. Cellular toxicity assay test

2.6.1. Morphology of cell

Cells from the minced animal's tissue were subjected to flow cytometry cell sorting. The crude cells were dissolved in 0.5 mL PBS. 100 µL of aliquots was redistributed to the BD flow cytometry tube. Results of the light scattering (forward/side scatter; FSC/SSC) were analyzed for at least 10,000 counts per sample in the flow cytometer. (FSC indicated cell morphology and SSC showed cell granularity).[58]

2.6.2. Cell viability

We used a rat model with a diabetic gingival wound to assess in vivo toxicity of $Ti_3C_2T_x$ MXene. We found that the IC50 of $Ti_3C_2T_x$ MXene was 34.83 µg/mL, aiming for 330 µg/mL in surgical tissue, and we used the IC50 for cellular toxicity factors (Fig. S1). Cells cultured from the minced rat diabetic gingival wound tissues were subjected to flow cytometry cell sorting based on cell morphology information (side scatter (SSC) and forward scatter (FSC)). The crude cells were dissolved in 0.5 mL of PBS. One hundred microliter aliquots were redistributed into BD flow cytometry tubes. The light scattering results were analyzed for at least 10,000 counts per sample using the flow cytometer.

Cell viability was evaluated by the MTT test. We prepare cells (1×10^4 cells/well) and incubated them in 96-well plates in a final volume of 50 ml. 20 mL of MTT was added to each well and then incubated for a supplementary 4h at 37 °C. The purple-blue MTT formazan precipitate was dissolved in 100 ml of DMSO and the absorbance at 570 nm was measured with an ELISA reader. Each test/group was examined with three replicates for each sample.[59]

2.6.3. Reactive Oxygen Species assay

In this experiment, isolated cells (1×10^6 cells), were placed in respiration buffer. Afterwards, 10 µM DCFH was added to the cellular suspension and then incubated for 15 min at 37 °C. In the next step, the fluorescence was measured using Shimadzu RF-5000U fluorescence spectrophotometer at the excitation and emission wavelengths of at $\lambda_{exitation}/\lambda_{emission}$ 488 nm /527 nm. Each group was examined with three replicates for each sample.[60]

View Article Online
DOI: 10.1039/D6TB00505E

2.6.4. Lipid Peroxidation (LPO) assay

The LPO was assayed by the determination of the amount of thiobarbituric acid reactive substances (TBARS) formed during the decomposition of lipid hydroperoxides on isolated cells (1×10^6 cells) by following the absorbance at 532 nm in an ELISA reader analyzer by determining the MDA level following the manufacturer's instructions. Each group was examined with three replicates for each sample.[61]

2.6.5. Protein carbonyl content assay

Protein was precipitated by adding an equal volume of 20% TCA and centrifuged on 11,000 g, 5 min. Cell (1×10^6 cells/well) were re-suspended in 10 mmol/L 2,4-dinitrophenylhydrazine solution for 15–30 min at room temperature before 20% TCA was added. The samples were centrifuged 11,000 g, 3 min. The carbonyl content was measured at 450 nm using ELISA reader. Each group was examined with three replicates for each sample.[62]

2.6.6. Glutathione assay

On isolated cells, (1×10^6 cells), reduced form glutathione Reductase (GSH) by OPA probe and glutathione Peroxidase form (GSSG) by NEM probe are the most important scavengers of ROS that can be utilized as a biomarker of the redox balance. Each sample was measured in quartz cuvettes using a Shimadzu RF-5000U fluorescence spectrophotometer set at $\lambda_{exitation}/\lambda_{emission}$ 350/420 nm wavelengths. Each group was examined with three replicates for each sample.[63]

2.6.7. Cytochrome c release assay

Cytochrome c release was determined at 450 nm according to the instructions provided by the manufacturer of the Kit. All analysis stages were carried out using an ELISA reader at desired concentrations in all groups. Each group was examined with three replicates for each sample.

2.6.8. Lysosome damage assay

Constancy of lysosome membrane was distinguished from the fluorescent dye redistribution and AO; hence, allocated cells (1×10^6 cells) suspension were stained by AO (5 μM) in which cells separated from the incubation plate by centrifugation with 1 min at 1000 rpm. As a result, the cells pellet replaced in 2 mL of fresh DMEM medium. The wash process was performed twice to remove the shiny fluorescent dye from the media. AO redistribution in the cell's suspension was

View Article Online
DOI: 10.1039/D6TB00505E

then measured Shimadzu RF-5000U fluorescence spectrophotometer set as $\lambda_{exitation}/\lambda_{emission}$ 490 and 535 nm. Each group was examined with three replicates for each sample.[64]

2.6.9. Apoptosis and Necrosis assay

After the treatment, the cells (1×10^6 cells) were stained with 5 ml of Annexin V and 5 ml of PI at room temperature for 20 min. The cells were diluted in the banding buffer (400 ml) and analyzed with flow cytometry. The fluorescence signals of Annexin V and PI were measured by flow cytometry on the FL1 and FL3 channels. Supplied with the software 1.2.5 and each determination was based on the mean fluorescence intensity of 10,000 counts and following the manufacturer's instructions.

2.7. Statistical Analysis

All statistical analyses were conducted using GraphPad Prism Software, version 10.0 (San Diego, CA, USA). The data are presented as mean ± standard deviation (SD). The Shapiro–Wilk test was employed to assess the normality of the data distribution. For experiments comparing the means of three or more independent groups, a One-Way Analysis of Variance (ANOVA) was performed initially. In cases where two independent factors were analyzed simultaneously (e.g., Treatment and Time), a Two-Way Analysis of Variance (ANOVA) was applied. To control for the Family-Wise Error Rate and to adjust P-values following the ANOVA, Tukey's post-hoc test was conducted for all necessary pairwise comparisons. Statistical significance for all tests was established using a threshold of $P < 0.05$.

3. Results and discussion

Diabetes mellitus (DM) is a significant global health burden, currently affecting approximately 463 million adults globally.[65] It is a long-term systemic metabolic condition characterized by defective insulin secretion and/or activity, resulting in sustained high blood glucose levels and multiple microvascular complications.[66] People with DM frequently experience various oral health issues, such as tooth loss, slow wound healing, dry mouth (xerostomia), dental decay, burning mouth syndrome, oral lichen planus, and, in advanced cases, bacterial osteomyelitis of the jaw. These manifestations often complicate dental management and can adversely affect treatment outcomes.[67] Hyperglycemia is closely linked to both systemic and oral health deterioration. Poor glycemic control compromises the immune response, particularly the function of neutrophils,

View Article Online
DOI: 10.1039/D6TB00505E

which are the body's primary defense against oral bacterial infections.[68] Evidence suggests that maintaining optimal blood glucose levels significantly reduces the risk of diabetes-associated complications, including those affecting oral health, as well as cardiovascular, neural, and ocular systems.

Individuals with diabetes often present a range of oral health disorders, the most common of which include bad breath (halitosis), impaired wound healing, dental cavities, dysfunction of the salivary glands, oral lichen planus, tongue lesions, various oral infections, and periodontal disease.[69] These complications are largely attributed to microvascular damage and sustained hyperglycemia. Epidemiological studies indicate that over 90% of individuals with DM develop oral health issues, and the prevalence of oral mucosal disorders is significantly higher among diabetic patients compared to non-diabetic populations.[70] With DM affecting roughly 8.5% of the global adult population, the burden of oral complications in this group warrants heightened clinical attention.[71] 2D nanomaterials possess exceptional properties, including high biocompatibility, potent antimicrobial effects, tunable phototherapeutic capabilities, and enhanced electrostimulation. These characteristics allow them to precisely modulate the wound microenvironment, leading to their widespread and successful application in tissue repair.[72] Thus, in this research, we studied the effect of $Ti_3C_2T_x$ MXene in gingival wound healing.

MXene was synthesized by selective etching of the aluminum (Al) layer from the Ti_3AlC_2 MAX phase. XRD analysis was used to investigate the structural properties of both the MAX phase and the resulting MXene (Fig. 1a). The diffraction pattern of the MAX phase exhibited sharp peaks at 2θ values of approximately 9.71° (002), 19.3° (004), and 39.10° (104), reflecting its well-ordered crystalline structure.[32] In contrast, the disappearance of the (104) peak and the shift and broadening of the (002) peak in the $Ti_3C_2T_x$ MXene confirmed the successful removal of the Al layer during the etching process. The morphology of MXene is shown in Fig. 1b Delaminated few-layer MXene sheets were obtained after sonication. Similar to graphene oxide,[73] the MXene flakes are wrinkled and curved at the edges.[32]

View Article Online
DOI: 10.1039/D6TB00505E

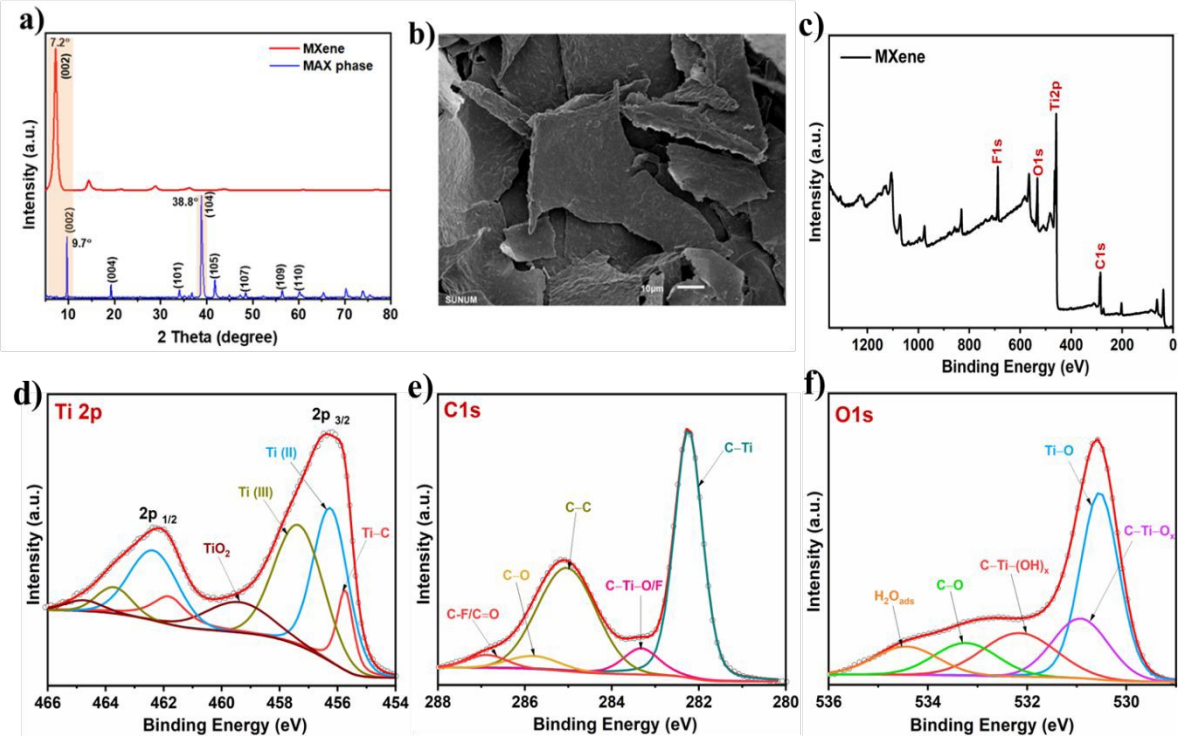

Fig. 1. a) The XRD patterns of MAX phase and MXene, b) SEM image of MXene, (c) the XPS survey scan of MXene, the high-resolution XPS spectra of d) Ti 2p, e) C 1s, f) O1s of MXene.

The XPS analysis was carried out to identify the surface species and corresponding chemical states of the MXene. The survey spectrum in Fig. 1c confirms the presence of Ti, C, O, and F signals.[37] The deconvoluted high-resolution spectra for Ti2p, C1s, and O1s are presented in Fig. 12d-f. Analysis of the $Ti2p_{3/2}$ ($2p_{1/2}$) region shows four doublets assigned to Ti–C, Ti(II), Ti(III), and TiO_2, with binding energies of 455.78 eV (461.88 eV), 456.28 eV (462.38 eV), 457.38 eV (463.78 eV), and 459.48 eV (464.78 eV), respectively.[32] The C1s spectrum is resolved into five components at 282.28 eV (C–Ti), 283.38 eV (C–Ti–O/F), 285.08 eV (C–C), 285.8 eV (C–O), and 286.88 eV (O–C=O). Similarly, the O1s envelope consists of peaks at 530.58 eV (Ti–O), 530.98 eV (C–Ti–O_x), 532.19 eV (C–Ti–$(OH)_x$), 533.28 eV (C–O), and 534.48 eV (adsorbed H_2O).

Dynamic light scattering (DLS) analysis showed that the hydrodynamic diameter of MXene was approximately 198 nm. The zeta potential measurements confirmed the high colloidal stability of the MXene which exhibited zeta potentials of -38.13 mV, consistent with their inherent negative surface charges.

In this study, we investigated the impact of $Ti_3C_2T_x$ MXene on oxidative stress pathways in fibroblast cells. Previous studies have explored the biocompatibility and safety of $Ti_3C_2T_x$ MXene

View Article Online
DOI: 10.1039/D6TB00505E

in various vivo models. For instance, Nasrallah et al. employed a zebrafish embryo model to evaluate the toxicity of $Ti_3C_2T_x$ nanosheets and reported that concentrations up to 50 μg/mL did not impair neuronal or muscular activity.[51] Zhang et al. implanted $Ti_3C_2T_x$ MXene films into subcutaneous tissues and calvarial defect sites in rats, followed by micro-CT imaging and histological analysis, revealing favorable bone regeneration and osteoinductive properties without evidence of toxicity or inflammation.[74] Li et al. synthesized $Bi_2S_3/Ti_3C_2T_x$ which exhibited excellent cytocompatibility and biocompatibility, promoted collagen fiber formation, and accelerated wound healing. Furthermore, the material's Schottky junction demonstrated outstanding biosafety in vivo [75]. Recently, Zahrabi et al. showed that melt electrowritten (3-aminopropyl)triethoxysilane-modified $Ti_3C_2T_x$/polycaprolactone 3D scaffold enhanced the osteogenic differentiation of MC3T3-E1 preosteoblast cells.[37]

A major obstacle in diabetic wound is the elevated susceptibility to bacterial and fungal infections around ulcerated regions, that can progress to severe complications such as foot amputation or even mortality. Multiple studies have shown that $Ti_3C_2T_x$ MXene possesses intrinsic antibacterial activity,[76] making it a promising candidate for diabetic ulcer management and the development of advanced wound dressings.

Hussein et al.[77] fabricated two $Ti_3C_2T_x$-based nanocomposites, Au/MXene and Au/Fe_3O_4/ MXene, and assessed their photothermal therapeutic performance in MCF-7 human breast cancer cells. Both composites demonstrated comparable photothermal efficacy; however, the hybrid nanocomposites exhibited reduced in vivo toxicity relative to pristine MXene. Acute toxicity studies in zebrafish embryos further indicated lower embryonic mortality for the composite materials. These findings suggest that surface modification and hybridization can enhance the biocompatibility of MXenes. Despite these advances, there remains a scarcity of comprehensive in vivo investigations assessing both short-term and long-term biosafety, underscoring the need for further preclinical validation before clinical translation.

Wojciechowska et al. investigated the effects of $Ti_3C_2T_x$/poly L-lactide flakes on human malignant melanoma cells (A375, ATCC) and human immortal keratinocytes (HaCaT). Their results demonstrated that concentrations up to 375 mg/L exhibited no cytotoxic effects.[78] Wang et al. coated $Ti_3C_2T_x$ films with silken protein and assessed cytotoxicity using human skin fibroblast HSAS1 cells. The silk fibroin-coated MXene maintained approximately 99% cell viability after six days of incubation that confirmed no significant reduction in viability, indicating enhanced biocompatibility of the coated films.[79]

View Article Online
DOI: 10.1039/D6TB00505E

As illustrated in the graph, HbA1c levels remained stable in the CH group (healthy control) throughout the 30-day period. In contrast, the CD group exhibited a progressive and statistically significant increase in HbA1c levels, peaking at approximately 12% by day 30. Statistical analysis indicates that the discrepancy between the groups reached a high level of significance (****P < 0.0001) from day 20 onwards, confirming the successful and sustained induction of the diabetic state in the study model. The elevated HbA1c levels in the CD group at the end of the 30 day period signify chronic dysregulation of glucose metabolism. Since HbA1c reflects the mean blood glucose concentration over a 2–3-month period, achieving a 12% threshold in this 30 day model not only confirms severe hyperglycemia but also establishes a rigorous environment for assessing wound healing interventions under high-oxidative stress conditions. These findings validate the robustness of the diabetic animal model for subsequent experimental phases (Fig. S1).

Blood glucose levels in the CH group remained relatively stable throughout the 28-day period (approximately ~110–125 mg/dL). In contrast, the CD group developed a time-dependent and statistically significant hyperglycemic shift starting at Day 7. Glucose levels increased to approximately ~250 mg/dL by Day 14 and then remained markedly elevated at ~260–280 mg/dL on Days 21 and 28. The significance markers (from **P < 0.0001 to ****P < 0.0001) indicate robust statistical differences across the corresponding time points, supporting a clear divergence between CH and CD over time. The temporal pattern observed in the CD cohort suggests successful establishment of hyperglycemia and persistent impairment of glycemic control. The onset of glucose elevation at Day 7, followed by attainment of high and sustained concentrations (~250–280 mg/dL) through Day 28, indicates that the diabetic phenotype is not merely transient but progresses toward a stable dysregulated state. From a model-validation perspective, these glucose measurements provide acute, high-resolution evidence of glycemic dysregulation, which when interpreted alongside long-term markers such as HbA1c strengthens the overall confirmation of the induced diabetic condition (Fig. S2).

To establish a biologically relevant concentration for subsequent studies, the cytotoxicity of $Ti_3C_2T_x$ MXene on standard fibroblast cells was quantified. Cells were treated with a concentration gradient of $Ti_3C_2T_x$ MXene ranging from 0 to 100 µg/mL (0, 2.5, 5, 10, 15, 20, 25, 30, 35, 40, 45, 50, 55, 60, 65, 70, 75, 80, 85, 90, 95, 100 µg/mL). Cell viability data were analyzed using nonlinear regression via software. This analysis determined the half-maximal inhibitory concentration (IC50) to be 34.83 ± µg/mL (wound surface area and target dose range 330 µg/mL after 72h) (Fig. S3)**.** Preliminary range-finding indicated that concentrations below 20 µg/mL showed minimal

View Article Online
DOI: 10.1039/D6TB00505E

cytotoxic effect, whereas doses exceeding 60 μg/mL resulted in severe cell death. Therefore, the calculated IC50 of 34.83 μg/mL was adopted as the standard concentration for assessing the biological effects of $Ti_3C_2T_x$ MXene in this study.

Wound dimensions were quantitatively evaluated using a caliper on days 0, 5, 15, and 30 days, following wound induction. Caliper measurements were applied in the early stage because the wound surface was still open and dynamically changing. As observed, the CH and CD groups showed neither wound cavity formation nor $Ti_3C_2T_x$ MXene exposure throughout the study period, resulting in negligible changes in macroscopic wound dimensions. In the CDD group, only wound cavity formation was evident. Since this group did not receive $Ti_3C_2T_x$ MXene treatment, the wound exhibited limited improvement in surface dimensions during the observation window. In contrast, the CDDM group demonstrated a clear healing trend, wound dimensions decreased progressively up to day 15, followed by complete recovery by day 30. Overall, these macroscopic results provide quantitative evidence that $Ti_3C_2T_x$ MXene enhances wound healing under diabetic conditions (Table. S4).

In our study in IC50, analysis of morphology (population~10000) using normal counts (Q_1), FSC (Q_2) and SSC (Q_1) for cells on days 0, 5, 15 and 30 were conducted. In Q_1 on day 0 in CH~97.07%, CD~80.69%, CDD~57.93%, CDDM~67.31%, on day 5 in CDDM~72.56%, on day 15 in CDDM~78.59%, and on day 30 in CDDM~86.81%. In Q_2 on day 0 in CH~0.13%, CD~16.86%, CDD~37.25%, CDDM~30.89%, on day 5 in CDDM~25.58%, on day 15 in CDDM~19.64%, and on day 30 in CDDM~11.71%. In Q_3 on day 0 in CH~2.27%, CD~2.09%, CDD~0.22%, CDDM~1.33% on day 5 in CDDM~0.94%, on day 15 in CDDM~1.46%, and on day 30 in CDDM~1.11% (Figure 2). The flow cytometric analysis of approximately 10,000 cells, assessing viability (Q_1), morphological changes (Q_2), and granularity changes (Q_3), revealed distinct temporal patterns within the study groups. Notably, the CDDM group exhibited a significant shift over 30 days. In Q_1 (viable cells area), CDDM showed a progressive increase from 67.31% on day 0 to 86.81% on day 30, indicating enhanced cell viability over time. Concurrently, CDDM demonstrated a decrease in Q_2 (changed shape cells area), dropping from 30.89% on day 0 to 11.71% on day 30, suggesting a reduction in cells undergoing morphological alteration. While Q_3 (changed granularity cells area) for CDDM fluctuated, it remained low, with a slight decrease from 1.33% on day 0 to 1.11% on day 30. These findings collectively suggest that the treatment promotes cell viability and a reduction in aberrant cellular morphology and granularity in the CDDM group by day thirty.

View Article Online
DOI: 10.1039/D6TB00505E

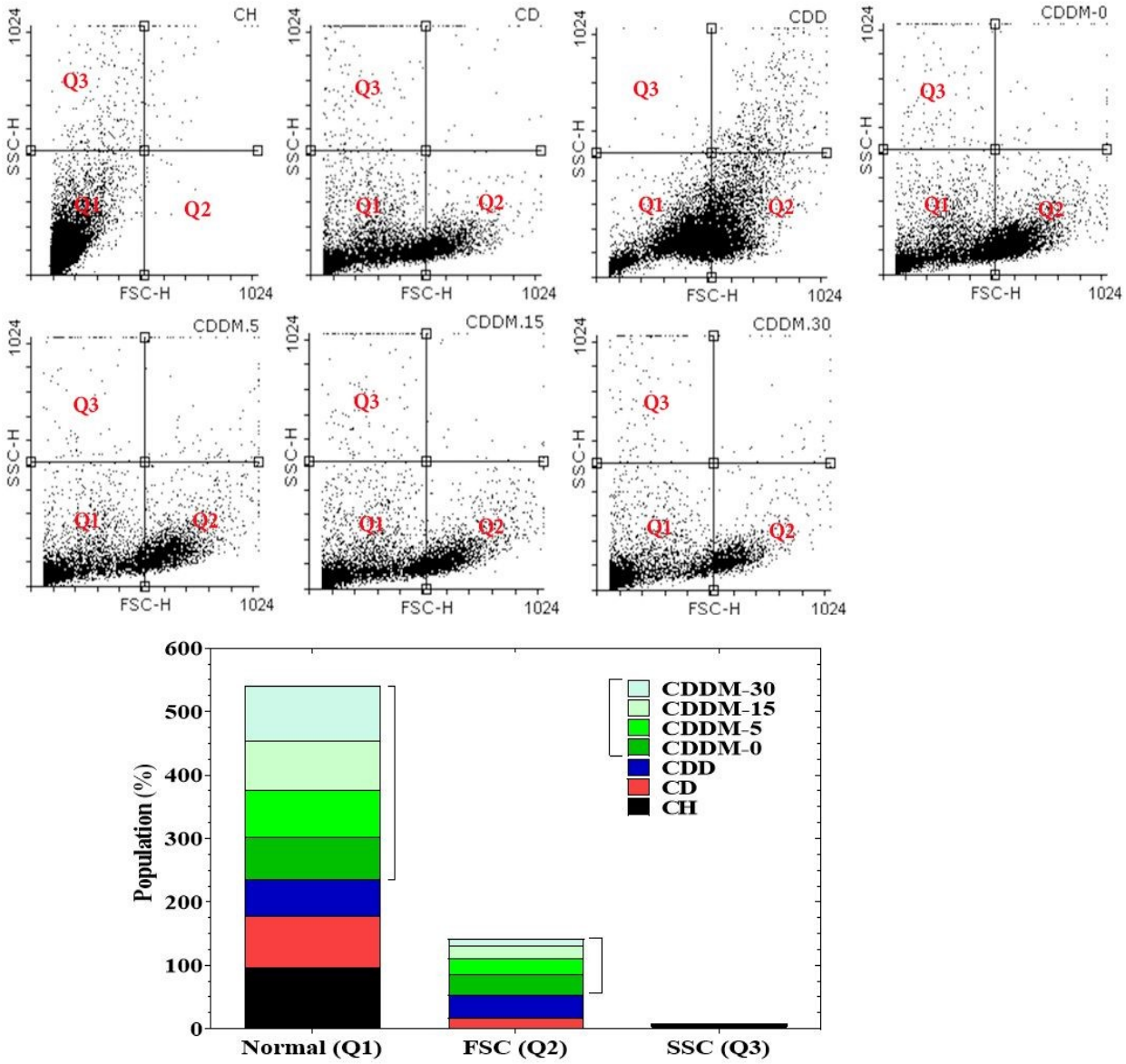

Fig. 2. Morphological analysis of the population of gingival cells (FSC/SSC) using Flow Cytometry.

As depicted in Fig. 3a, cell viability showed a slight yet significant decrease on day 0 in the CDD group (*P<0.05) and a more pronounced reduction in the CDDM group (****P<0.0001). Subsequently, from day 5 onward, a notable decline in cell viability was observed in the CDD and CDDM groups (****P<0.0001). This decreasing trend continued until day 15, with significant reductions noted in the CD, CDD and CDDM groups (****P<0.0001). By day 30, cell viability had further decreased in the CD and CDD groups (****P<0.0001). Interestingly, on the same day,

View Article Online
DOI: 10.1039/D6TB00505E

an increase in cell viability was registered in the CDDM group (*P<0.05) compared to the control healthy group (CH).

Our results showed that $Ti_3C_2T_x$ MXene treatment reduced ROS levels and improved fibroblast viability (CDDM) over 30 days period (Fig. 3b). This finding aligns with the observations of Song et al.[80] who reported that diabetic wound microenvironments often produce excessive ROS due to activation of oxidative stress pathways, resulting in decreased cell survival. Biochemically, succinate dehydrogenase plays a crucial role in the mitochondrial electron transport chain, where it catalyzes the conversion of succinate to fumarate, accompanied by the reduction of flavin adenine dinucleotide (FAD) to its reduced form, flavin adenine dinucleotide dehydrogenated ($FADH_2$). The resulting electrons are transferred through the respiratory chain to oxygen, regenerating FAD. This enzymatic activity serves as an important indicator of mitochondrial function and oxidative metabolism. In our research, on days 0 and 5, significantly elevated levels of ROS were detected in the CDDM, CDD, and CD groups (****P<0.0001). On day 15, an increase was observed in the CD and CDD groups (****P<0.0001), whereas the CDDM group (**P<0.01) showed a decrease. By day 30, substantial increases were observed in the CD and CDD groups (****P<0.0001), while the CDDM group showed an opposite trend, suggesting a potential mitigating or stabilizing effect of the MXene treatment over the longer term (Fig. 3b). All these observed increases in ROS levels across days 0, 5, 15, and 30 were consistently compared against the control healthy group (CH). The results in the CDDM group indicate the role of $Ti_3C_2T_x$ MXene in decreasing the level of ROS (Figure 3b). By attenuating ROS production, a strong correlation was observed between $Ti_3C_2T_x$ MXene exposure and alterations in key components of the cell death signaling pathway, suggesting a potential regulatory role in fibroblasts and support cell survival, even under prolonged exposure. Collectively, our results suggest that $Ti_3C_2T_x$ MXene exerts protective effects against oxidative stress; thereby enhancing cell viability in wound-healing contexts, particularly within diabetic gingival wound in rat models.

Pierce et al.[81] reported that ROS promote lipid and protein peroxidation in diabetic wound tissues, thereby activating multiple inflammatory and oxidative stress pathways, including interleukin-1β (IL-1β), tumor necrosis factor-α (TNF-α), cytokines, nuclear factor erythroid 2–related factor 2 (Nrf-2), and nuclear factor kappa B (NF-κB). Tiwari et al.[82] further demonstrated a significant clinical association between lipid peroxidation and hyperglycemia, with higher fasting blood glucose and elevated glycated hemoglobin/fasting plasma glucose (HbA1c/FPG) ratios correlating strongly with increased oxidative stress in diabetic patients. ROS-mediated lipid membrane

View Article Online
DOI: 10.1039/D6TB00505E

oxidation is believed to disrupt the mitochondrial electron transport chain, initiating cell death signaling cascades.

As shown in Fig. 3c, the MDA levels, that indicate a significant increase in lipid peroxidation Compared to the control healthy (CH) group, significant changes were observed in the CD, CDD and CDDM groups. Specifically, on days 0 and 5, the CD, CDD, and CDDM groups showed alterations (****P<0.0001) compared with the CH group. After 15 days, the CD and CDD groups continued to display a highly significant increase (****P<0.0001), and the CDDM group also presented a dramatic change (*P<0.05) when compared to the CH group. Furthermore, our findings indicated a slight but statistically significant decrease in lipid peroxidation levels within the CDDM group after 30 days.

Despite this reduction, it was not sufficient to prevent cell injuries. In our study, lipid peroxidation was assessed by measuring thiobarbituric acid reactive substances (TBARS) formation in fibroblasts exposed to $Ti_3C_2T_x$ MXene (Fig. 3c). After 30 days, fibroblasts in the $Ti_3C_2T_x$ MXene-treated group exhibited markedly reduced lipid peroxidation compared to CH, indicating a protective effect against oxidative membrane damage.

The data in Fig. 3d, showed that protein carbonyl levels significantly increased in the CD (**P<0.01), CDD and CDDM (****P<0.0001) groups, and marked cell injuries occurred in diseased cells compared to the CH group on day 0. On day 5, protein carbonyl levels increased in the CD (***P<0.001), CDD, and CDDM (****P<0.0001) groups compared to the CH group. On day 15, protein carbonyl levels significantly increased in the CD and CDD groups (****P<0.0001), whereas levels decreased in the CDDM group (***P<0.001) compared to the CH group. On day 30, protein carbonyl levels significantly increased in the CD and CDD groups (****P<0.0001), while the CDDM group showed no significant change compared to the control group.

Their findings emphasized that therapeutic strategies targeting precise modulation and control of inflammation during the healing process may offer considerable benefits for managing diabetic and other chronic wounds. The observed malondialdehyde (MDA) levels were strongly associated with ROS generation and consequent lipid membrane damage. Likewise, the increase in protein carbonyl content likely reflects oxidative modification of cellular proteins by elevated ROS, a process considered a critical indicator of oxidative stress and frequently linked to loss of protein function.[26] In fibroblast cells exposed to $Ti_3C_2T_x$ MXene for 30 days, carbonyl protein levels remained markedly lower compared with the CD group (Fig. 3d). As highlighted by Boniakowski

View Article Online
DOI: 10.1039/D6TB00505E

et al. elevated ROS not only contributes to the onset and progression of diabetic wounds, but also intensifies the inflammatory response, thereby impairing tissue repair and reducing the efficacy.

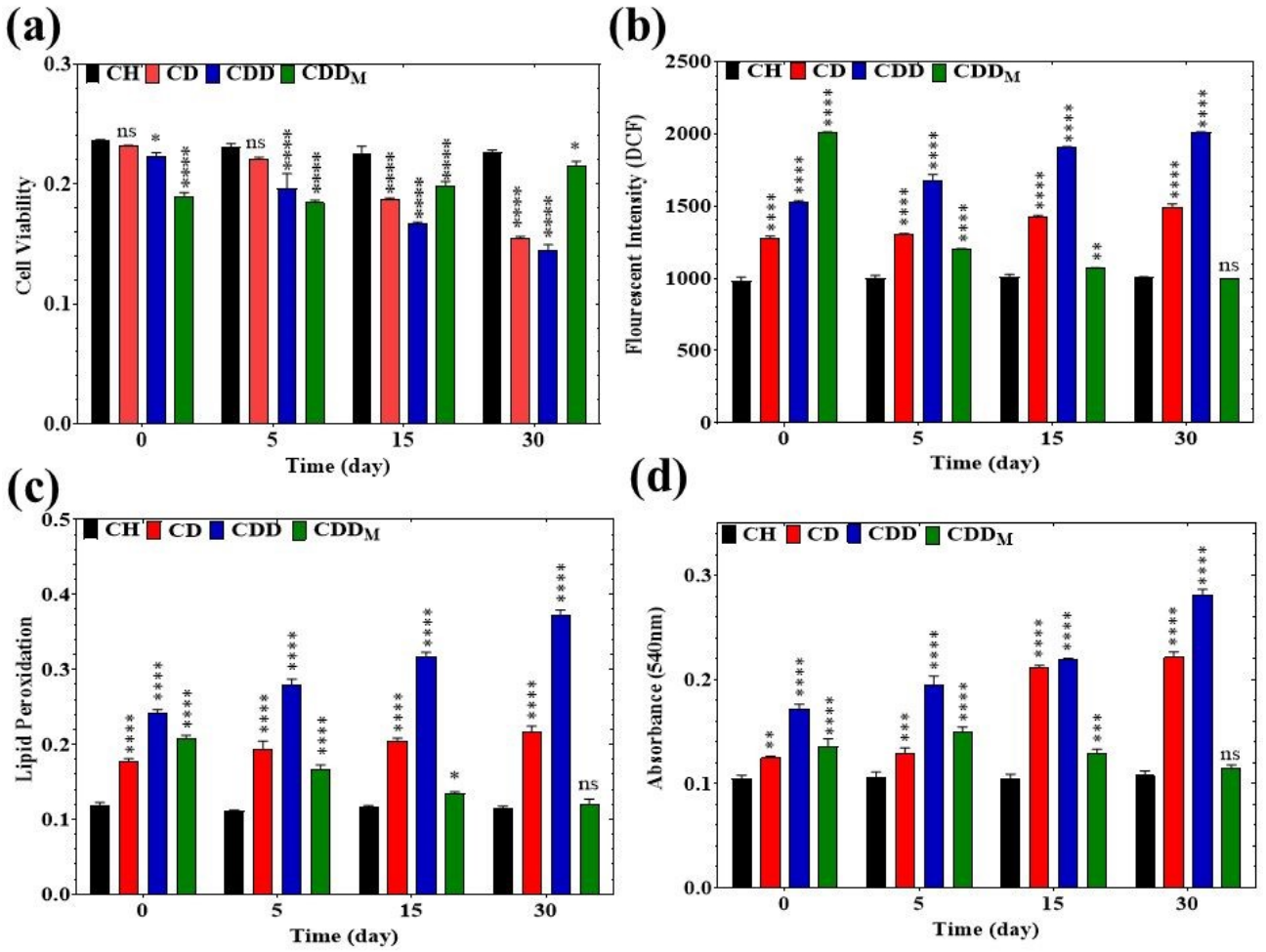

Fig. 3. a) Detection of cell viability, **b)** Detection of Reactive oxygen species (ROS), **c)** Detection of lipid peroxidation (LPO), **d)** Detection of carbonyl protein content on control health (CH), control diabetic (CD), diabetic and surgical gingivae (CDD), and diabetic, surgical gingivae and treated by $Ti_3C_2T_x$ MXene (CDDM) in fibroblast cell after 0, 5, 15 and 30 days. Data represented as mean ± SD of data determined from three separate experiments. Values represented as mean ± SD (n = 5). ns=no significant, *P < 0.05 and ****P < 0.0001 compared with the control health (CH) group.

A previous study[82] showed that GSH serves as a key cellular antioxidant defense, capable of directly interacting with ROS in non-enzymatic reactions, resulting in its oxidation to GSSG. GSSG can negatively impact cells through two primary pathways: it may function as a toxic compound by forming conjugates with cellular proteins, or it can be converted back to its reduced

View Article Online
DOI: 10.1039/D6TB00505E

form by glutathione reductase before being either exported via glutathione S-transferase or involved in nonenzymatic adduct formation.

Fig. 4a illustrates the content of reduced GSH. On days 0 and 5, significant differences were observed in the CD, CDD and CDDM groups (****P<0.0001) compared to the control healthy (CH) group. On days 15 and 30, the CD and CDD groups exhibited a significant decrease in GSH content (****P<0.0001), while the CDDM group also showed significant reductions (**P<0.01 and *P<0.05, respectively) relative to the CH group. A slight decrease was also noted in the CDDM group on these later days compared to the other diseased groups.

On days 0 and 5, significant differences were observed in the CD, CDD, and CDDM groups (****P<0.0001) compared to the control healthy (CH) group. On days 15 and 30, the CD and CDD groups exhibited a significant decrease in GSH content (****P<0.0001), indicating a sustained state of oxidative stress, while the CDDM group also showed a significant reduction (**P<0.01) after 15 days. However, the CDDM group did not show a significant change on day 30.

As illustrated in Fig. 4a, b, exposure to $Ti_3C_2T_x$ MXene led to changes in the levels of both GSH and GSSG in fibroblasts from the gingival tissue of diabetic animals. Glutathione is recognized as a vital cellular antioxidant, with its GSH capable of directly neutralizing ROS through nonenzymatic reactions, resulting in its oxidation to GSSG. The GSSG can be detrimental to cells by acting as a toxic compound, forming conjugates with proteins, or participating in nonenzymatic adduct formation. Alternatively, it can be recycled back to GSH via GSSG before being exported from the cell through glutathione S-transferase.[83] In several pathological conditions, including diabetes and various cancers, apoptosis serves as a fundamental mechanism of cell death, characterized by features such as cell shrinkage, nuclear fragmentation, chromatin condensation, and double-stranded DNA fragmentation, whereas necrosis is typically associated with cell membrane damage. Apoptosis is a tightly controlled cellular mechanism initiated by intracellular signaling pathways in response to stress conditions like elevated glucose levels, oxygen deprivation, or increased temperature, ultimately resulting in programmed cell death. According to Saelens et al.[84] mitochondrial swelling disrupts the configuration of the mitochondrial permeability transition (MPT) pore, leading to the release of pro-apoptotic molecules such as cytochrome c, Smac/DIABLO, and the serine protease HtrA2/Omi.[85]

View Article Online
DOI: 10.1039/D6TB00505E

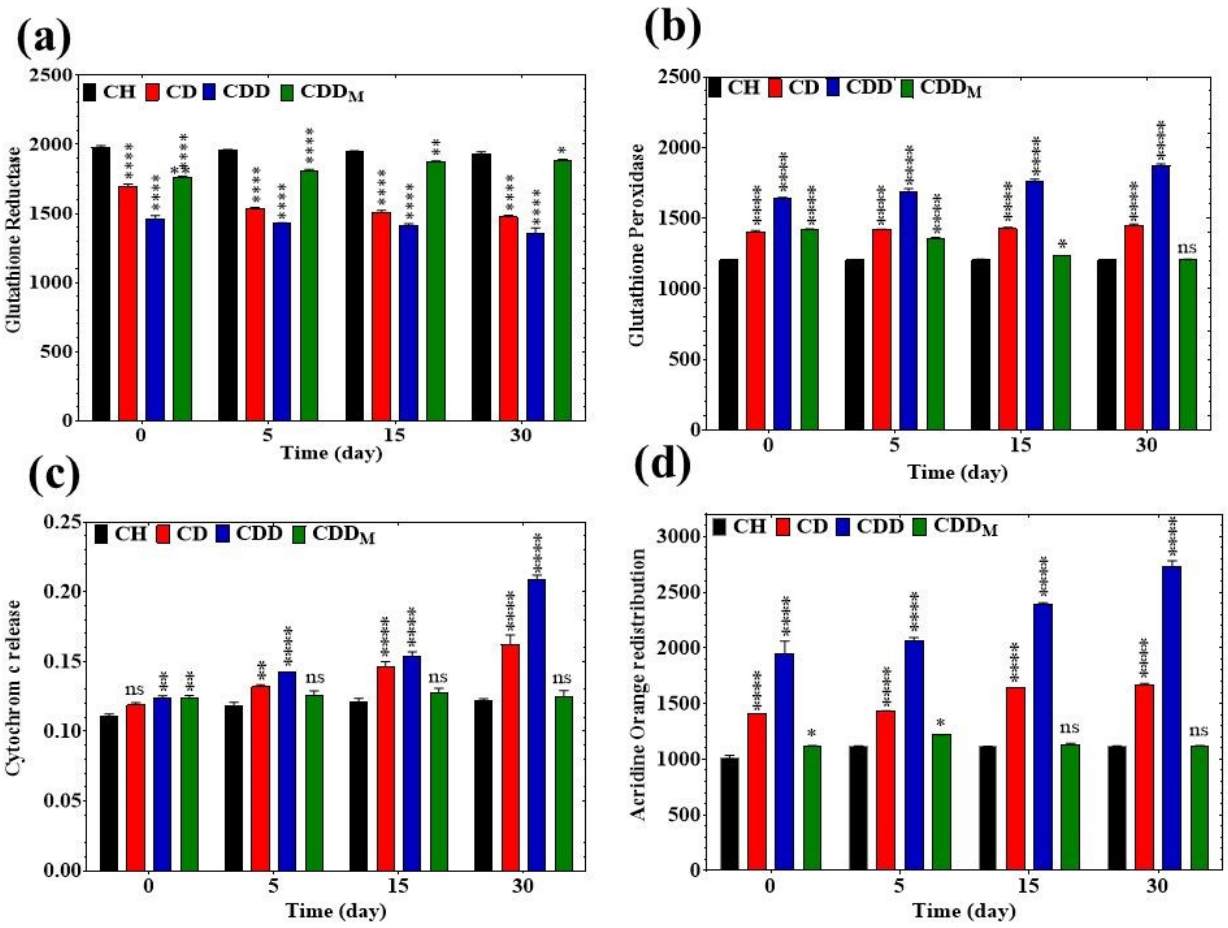

Fig. 4. a) Detection of Glutathione Reductase (GSH), **b)** Detection of Glutathione Peroxidase (GSSG), **c)** Detection of release cytochrome c, **d)** Detection of lysosomal membrane damage on control health (CH), control diabetic (CD), diabetic and surgical gingivae (CDD), and diabetic, surgical gingivae and treated by $Ti_3C_2T_x$ MXene (CDDM) in fibroblast cell after 0, 5, 15 and 30 days. Data represented as mean ± SD of data determined from three separate experiments. Values represented as mean ± SD (n = 5). ns=no significant, *P < 0.05; **P < 0.01 and ****P < 0.0001 compared with the control health (CH) group.

Figure 4c details the release of cytochrome c. On day 0, a slight increase in cytochrome c release was observed in the CDD and CDDM groups (**P<0.01) relative to the CH group. On day 5, a slight increase in cytochrome c release was observed in the CD (**P<0.01) and CDD (****P<0.0001) groups relative to the CH group. However, by days 15 and 30, the pattern of release had evolved significantly. A dramatic increase in cytochrome c release was noted in the CD and CDD groups (****P<0.0001). In contrast, the CDDM group showed no increase compared to the CH group on days 5, 15, and 30. Permeabilization of the mitochondrial outer membrane

View Article Online
DOI: 10.1039/D6TB00505E

triggers the release of cytochrome c from the intermembrane space, a critical event in the initiation of cell death. Cytochrome c, carrying a strong positive charge, binds to negatively charged lipids on the outer surface of the inner mitochondrial membrane. This release is closely linked to ROS production. Our findings showed that exposure to $Ti_3C_2T_x$ MXene reduced the release of cytochrome c into the cytoplasm of fibroblasts in CDDM group. In contrast, the diabetic control group exhibited pronounced mitochondrial outer membrane permeabilization facilitating substantial cytochrome c release from the intermembrane space.[84]

The release of cytochrome c into the cytoplasm is a key step in triggering the activation of caspases. Once there, with the help of Apoptotic Protease Activating Factor-1 (Apaf-1) and ATP, cytochrome c recruits pro-caspase-9. This forms a complex called the apoptosome which then activates caspase-9. The activated caspase-9 subsequently activates the downstream effectors caspase-3. Moreover, proteins like Smac/DIABLO and HtrA2/Omi promote apoptotic cell death by suppressing the activity of Inhibitor of Apoptosis Proteins (IAPs).[86]

Exposure to ROS can compromise the integrity of lysosomes by causing lipid peroxidation of their membranes. The resulting proton leakage leads to lysosomal alkalinization, which is believed to contribute to many diseases because a proper acidic pH is crucial for lysosomal function. Consequently, strategies to restore lysosomal pH, either through compensatory biological responses or therapeutic interventions, are expected to offer significant benefits. Interestingly, it is worth noting that not all lysosomes respond to oxidative stress in the same way or even maintain the same luminal pH.[87]

Figure 4d illustrates the level of lysosomal damage. A statistical difference in lysosomal damage was observed between the control healthy (CH) group and the CD, CDD (****$P<0.0001$), and CDDM (*$P<0.05$) groups after 0 and 5 days. Furthermore, over the 15- and 30-days period, a dramatic increase in lysosomal damage was evident in both the CD and CDD groups (****$P<0.0001$) compared to the CH group. No lysosomal damage was observed in the CDDM group compared to the CH group.

Apoptosis is an essential cellular mechanism involved in the progression of various diseases, including diabetes and cancer. It is defined by specific morphological changes such as cell contraction, chromatin condensation, nuclear fragmentation, and the cleavage of double-stranded DNA. Unlike necrosis, which is marked by membrane rupture and cell lysis, apoptosis follows a

View Article Online
DOI: 10.1039/D6TB00505E

regulated pathway. This process is generally initiated by intracellular stressors such as elevated glucose levels, oxygen deprivation, or heat stress, ultimately leading to programmed cell death.[88] Analysis of apoptosis/necrosis pathways using annexin V/PI double staining the apoptosis was quantified by the externalization of phosphatidylserine (PS). PI (stains the nuclear) was used as an indicator of membrane integrity at 0, 5, 15 and 30 days. The results showed cell death signaling. The cell viability counts (Q_1) on 0 day in CH~99.67%, CD~99.37%, CDD~29.26%, CDDM~57.48%, on day 5 in CH~99.50%, CD~82.86%, CDD~23.3%, CDDM~73.38%, on day 15 in CH~99.13%, CD~79.63%, CDD~12.97%, CDDM~84.29%, and on day 30 in CH~98.65%, CD~ 75.52%, CDD~8.42%, CDDM~92.13%. The necrotic cell counts (Q_2) on day 0 in CH~0.13%, CD~0.10%, CDD~5.14%, CDDM~21.36%, on day 5 in CH~0.11%, CD~8.37%, CDD~21.39%, CDDM~9.97%, on day 15 in CH~0.12%, CD~19.91%, CDD~16.09%, CDDM~0.10%, on day 30 in CH~0.12%, CD~23.72%, CDD~15.82%, CDDM~2.65%. The early apoptotic cell counts (Q_3) on day 0 in CH~0.12%, CD~0.29%, CDD~47.27%, CDDM~14.66%, on day 5 in CH~0.19%, CD~5.07%, CDD~55.27%, CDDM~0.76%, on day 15 in CH~0.34%, CD~0.08%, CDD~68.51%, CDDM~1.62%, on day 30 in CH~0.30%, CD~0.50%, CDD~75.28%, CDDM~4.62%. The late apoptotic cell counts (Q_4) on day 0 in CH~0.08%, CD~ 0.24%, CDD~18.18%, CDDM~6.39%, on day 5 in CH~0.20%, CD~ 3.27%, CDD~0.19%, CDDM~5.71%, on day 15 in CH~0.4%, CD~0.00%, CDD~2.38%, CDDM~13.93%, and on day 30 in CH~0.93%, CD~0.00%, CDD~0.47%, CDDM~0.58% (Fig. 5).

Apoptosis was quantified by phosphatidylserine (PS) externalization and assessed using annexin V/propidium iodide (PI) double staining on day 0, 5, 15, and 30. PI, which stains the nucleus, served as an indicator of membrane integrity, allowing differentiation between apoptotic and necrotic cells. The current findings reveal that exposure to $Ti_3C_2T_x$ MXene showed a notable association with variations in apoptosis-related signaling rather than direct modulation of these pathways. Apoptosis is a fundamental biological process contributing to the resolution of inflammation and guiding the transition of granulation tissue toward mature scar formation during wound healing. In the context of diabetes, compromised wound healing continues to pose a major clinical concern, predominantly linked to disrupted apoptotic homeostasis resulting from inadequate glycemic regulation. The observed correlation between $Ti_3C_2T_x$ MXene presence and apoptosis-associated responses highlights a promising avenue for further investigation into its potential implications for enhancing wound-healing dynamics under diabetic conditions.

View Article Online
DOI: 10.1039/D6TB00505E

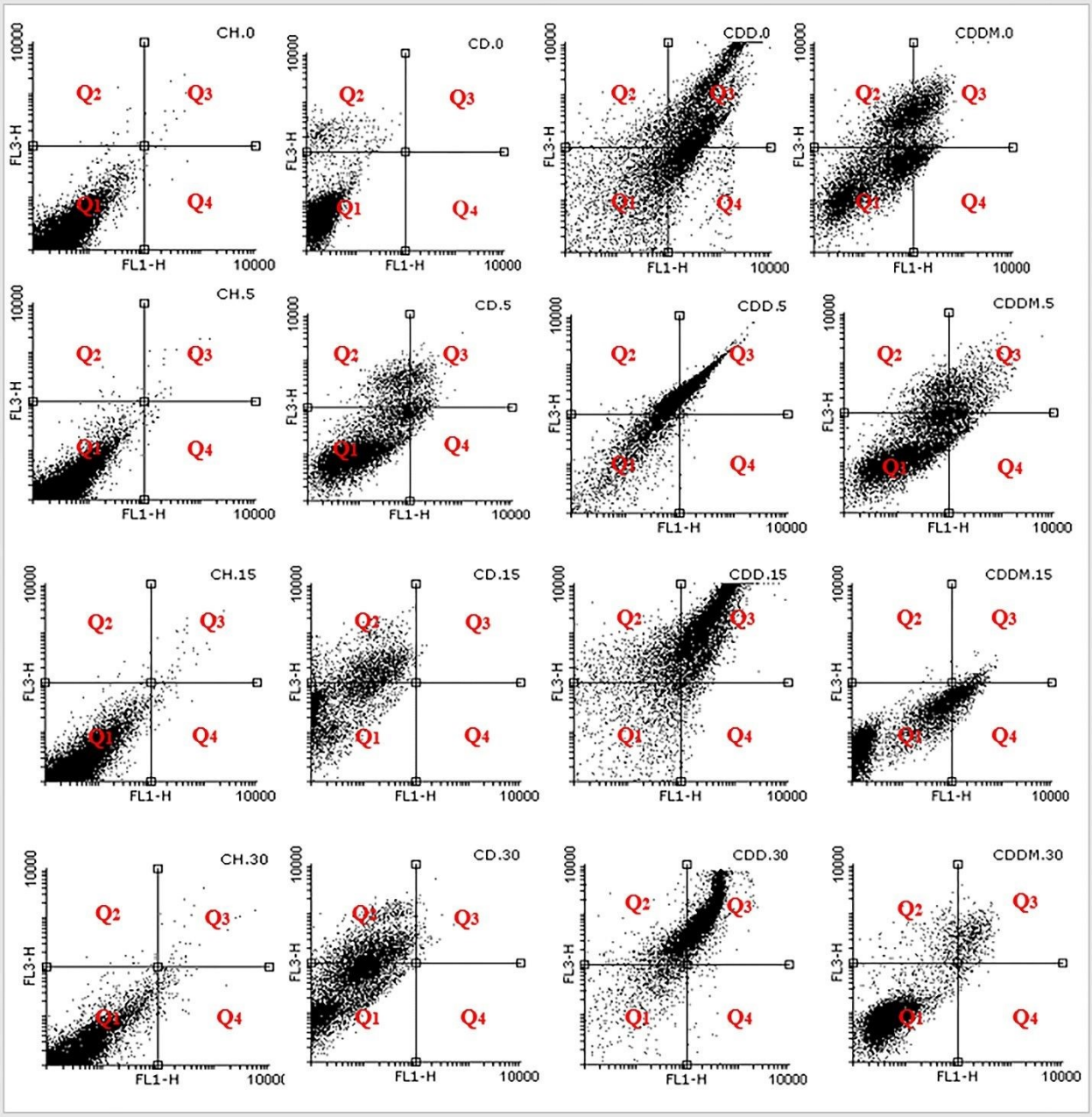

Fig. 5. Effect of $Ti_3C_2T_x$ MXene on apoptosis and necrosis. Detection of apoptosis/necrosis pathways using annexin V/PI double staining the apoptosis was quantified by the externalization of phosphatidylserine (PS). PI (stains the nuclear) was used as an indicator of membrane integrity on day 0, 5, 15 and 30 in control health (CH), control diabetic disease (CD), diabetic diseases and surgical tooth gum (CDD), and diabetic diseases and surgical gingiva and treatment by $Ti_3C_2T_x$ MXene (CDDM) in fibroblast cell. Data represented as mean ± SD of data determined from three separate experiments. Values represented as mean ± SD (n = 5). ns=no significant, *P < 0.05; **P < 0.01 and ***P < 0.001 compared with the control health (CH) group.

View Article Online
DOI: 10.1039/D6TB00505E

Conclusion

The present study demonstrated that $Ti_3C_2T_x$ MXene exhibits noteworthy biocompatibility and shows a clear association with well-regulated cellular and mitochondrial responses in fibroblast cells derived from abnormal gingival tissue of diabetic animal models. The experimental evidence revealed correlations between $Ti_3C_2T_x$ MXene exposure and controlled oxidative stress, sustained cell viability, and lowered intracellular ROS levels. These relationships were accompanied by preservation of glutathione balance, stabilization of mitochondrial membrane potential, and moderation of cytochrome c–associated caspase activation, collectively aligning with a more regulated apoptotic profile in abnormal cells. Taken together, the findings support further investigation of $Ti_3C_2T_x$ MXene as a potentially valuable candidate for developing advanced nano-enabled therapeutic formulations such as topical medicines, gels, creams, or powders aimed at improving wound healing in diabetic conditions. Furthermore, integration of such approaches into proactive oral healthcare frameworks, supported by interdisciplinary collaboration, may contribute to enhanced oral health outcomes among diabetic patients.

Data availability statement

The authors declare that the data supporting the findings of this study are available within the paper and its Supplementary Information file.

Declaration of Competing Interest

The authors declare that they have no competing financial interests or personal relationships that could have appeared to influence the work reported in this paper.

Funding Declaration

This work was financially supported by FLAG-ERA grant [GRAPH-OCD], by the Scientific and Technological Research Council of Turkey (TUBITAK) [223N171].

Author Contributions

PN: conceptualization, investigation, methodology, characterizations, data management, validation, visualization, original draft preparation, review and editing, resources. MN: conceptualization, investigation, methodology, characterizations, data management, validation, visualization, original draft preparation, review and editing, resources. AR: original draft

View Article Online
DOI: 10.1039/D6TB00505E

preparation, review and editing. SA: original draft preparation, characterizations, data management, review and editing.

References

1. S. A. J. Mossavi, J. F. Ramandi, F. Ghanbary, N. Hosseini, P. Naserzadeh, M. Akhshik, F. R. Tay and B. Ashtari, Nano, 0, 2450047.
2. M. Brownlee, Nature, 2001, 414, 813-820.
3. G. L. King, Journal of periodontology, 2008, 79, 1527-1534.
4. E. Lalla and P. N. Papapanou, Nature Reviews Endocrinology, 2011, 7, 738-748.
5. W. S. Borgnakke, P. V. Yl€ ostalo, G. W. Taylor and R. J. Genco, Journal of periodontology, 2013, 84, S135-S152.
6. T. C. Simpson, J. C. Weldon, H. V. Worthington, I. Needleman, S. H. Wild, D. R. Moles, B. Stevenson, S. Furness and Z. Iheozor-Ejiofor, Cochrane Database of Systematic Reviews, 2015.
7. O. Z. Lerman, R. D. Galiano, M. Armour, J. P. Levine and G. C. Gurtner, The American journal of pathology, 2003, 162, 303-312.
8. V. Falanga, The Lancet, 2005, 366, 1736-1743.
9. M. Christgau, K. D. Palitzsch, G. Schmalz, U. Kreiner and S. Frenzel, Journal of clinical periodontology, 1998, 25, 112-124.
10. L. Kardeşler, N. Buduneli, Ş. Çetinkalp, D. Lappin and D. F. Kinane, Inflammation Research, 2011, 60, 143-151.
11. J. Katz, I. Bhattacharyya, F. Farkhondeh-Kish, F. Perez, R. Caudle and M. Heft, Journal of clinical periodontology, 2005, 32, 40-44.
12. B. L. Mealey and T. W. Oates, Journal of periodontology, 2006, 77, 1289-1303.
13. P. Palumbo and L. J. MELTON III, Diabetes in America, 1995, 401.
14. J. P. Yadav, D. K. Patel, A. Verma and P. Pathak, Obesity Medicine, 2024, 47, 100535.
15. E. H. Espensen, B. P. Nixon, L. A. Lavery and D. G. Armstrong, Journal of the American Podiatric Medical Association, 2002, 92, 395-397.
16. Y. Teng, Y. Li, J. Wang, K. Yang, Y. Zhang, Y. Wang, J. Tian, B. Ma, J. Wang and X. Yan, Diabetes, Obesity and Metabolism, 2010, 12, 307-315.
17. L. Chen, P. Wu, Y. Zhu, H. Luo, Q. Tan, Y. Chen, D. Luo and Z. Chen, APL bioengineering, 2025, 9.
18. M. Mir, M. N. Ali, A. Barakullah, A. Gulzar, M. Arshad, S. Fatima and M. Asad, Progress in biomaterials, 2018, 7, 1-21.
19. W. S. Tan, P. Arulselvan, S.-F. Ng, C. N. Mat Taib, M. N. Sarian and S. Fakurazi, BMC complementary and alternative medicine, 2019, 19, 20.
20. A. Montaser, A. Abdel-Mohsen, M. Ramadan, A. Sleem, N. Sahffie, J. Jancar and A. Hebeish, International journal of biological macromolecules, 2016, 92, 739-747.
21. L. Hou, X. Zhang and H. Du, Diabetes/Metabolism Research and Reviews, 2023, 39, e3638.
22. M. Namvari, C. S. Biswas, Q. Wang, W. L. Liang and F. J. Stadler, Journal of Colloid and Interface Science, 2017, 504, 731-740.
23. G. M. Choi, M. Park, Y. H. Shim, S. Y. Kim, M. Namvari and H. S. Lee, Advanced Functional Materials, 2022, 32, 2202564.
24. A. Altan and M. Namvari, 2D Materials, 2023, 10, 042001.
25. A. Bahadoran, N. Ajinkya, M. Sharghi, F. Hasanvandian, Y. Wang, H. Chen, M. Namvari, B. Kakavandi, E. Marsili, M. Galluzzi and S. Ramakrishna, Journal of Materials Chemistry A, 2024, 12, 14619-14635.
26. V. Vijayakumar, S. K. Samal, S. Mohanty and S. K. Nayak, International Journal of Biological Macromolecules, 2019, 122, 137-148.

View Article Online
DOI: 10.1039/D6TB00505E

27. M. Namvari and B. K. Chakrabarti, Advances in Colloid and Interface Science, 2024, 331, 103208.
28. R. Afshar Ghotli, M. Namvari and B. K. Chakrabarti, Advanced Materials Technologies, n/a, e01403.
29. M. Naguib, M. Kurtoglu, V. Presser, J. Lu, J. Niu, M. Heon, L. Hultman, Y. Gogotsi and M. W. Barsoum, in *MXenes*, Jenny Stanford Publishing, 2023, pp. 15-29.
30. M. Namvari, T. Inan and A. Altan, Graphene and 2D Materials, 2023, 8, 5-26.
31. A. Ben Ayed and M. Namvari, Advanced Composites and Hybrid Materials, 2025, 8, 410.
32. A. Güngör, M. Namvari, A. B. Ayed and E. Erdem, Small, 2025, n/a, e05698.
33. R. Afshar Ghotli, Z. Kudaş, R. Zaidi, K. B. Dönmez, Z. Çobandede, A. Ben Ayed, M. Namvari, B. Alkhateab, S. Çelik, F. S. Mjalli, T. Y. İnan, M. K. Bayazıt, S. H. Soytaş, N. P. Brandon and B. K. Chakrabarti, ChemCatChem, n/a, e01280.
34. A. Ben Ayed, M. Masoudi and M. Namvari, FlatChem, 2026, 57, 101052.
35. M. Soleymaniha, M.-A. Shahbazi, A. R. Rafieerad, A. Maleki and A. Amiri, Advanced Healthcare Materials, 2019, 8, 1801137.
36. Z. Liu, C. Sun, M. Xu and W. Huang, Materials Letters, 2024, 365, 136437.
37. M. Zahrabi, M. Altunbek, S. Celik, M. Namvari and B. Koc, Biofabrication, 2025, https://doi.org/10.1088/1758-5090/adf803.
38. Y. He, H. Sun, Y. Wang, Y. n. Yu, C. Mu and L. Chen, Chemical Engineering Journal, 2024, 485, 150047.
39. Z. K. Li, Y. Wei, X. Gao, L. Ding, Z. Lu, J. Deng, X. Yang, J. Caro and H. Wang, Angewandte Chemie International Edition, 2020, 59, 9751-9756.
40. H. Lin, X. Wang, L. Yu, Y. Chen and J. Shi, Nano Letters, 2017, 17, 384-391.
41. C. Dai, H. Lin, G. Xu, Z. Liu, R. Wu and Y. Chen, Chemistry of Materials, 2017, 29, 8637-8652.
42. G. Liu, J. Zou, Q. Tang, X. Yang, Y. Zhang, Q. Zhang, W. Huang, P. Chen, J. Shao and X. Dong, ACS applied materials & interfaces, 2017, 9, 40077-40086.
43. X. Han, J. Huang, H. Lin, Z. Wang, P. Li and Y. Chen, Advanced healthcare materials, 2018, 7, 1701394.
44. C. Yang, D. Xu, W. Peng, Y. Li, G. Zhang, F. Zhang and X. Fan, Nanoscale, 2018, 10, 15387-15392.
45. H. Vojoudi and M. Soroush, Advanced healthcare materials, 2025, 14, 2500359.
46. G. P. Lim, C. F. Soon, N. L. Ma, M. Morsin, N. Nayan, M. K. Ahmad and K. S. Tee, Environmental research, 2021, 201, 111592.
47. J. Liu and C. N. Pope, in *An Introduction to Interdisciplinary Toxicology*, Elsevier, 2020, pp. 285-293.
48. B. e. Scheibe, J. K. Wychowaniec, M. Scheibe, B. Peplińska, M. Jarek, G. Nowaczyk and Ł. Przysiecka, ACS biomaterials science & engineering, 2019, 5, 6557-6569.
49. A. Jastrzębska, A. Szuplewska, T. Wojciechowski, M. Chudy, W. Ziemkowska, L. Chlubny, A. Rozmysłowska and A. Olszyna, Journal of hazardous materials, 2017, 339, 1-8.
50. A. Jastrzębska, A. Szuplewska, A. Rozmysłowska-Wojciechowska, M. Chudy, A. Olszyna, M. Birowska, M. Popielski, J. A. Majewski, B. Scheibe and V. Natu, 2D Materials, 2020, 7, 025018.
51. G. K. Nasrallah, M. Al-Asmakh, K. Rasool and K. A. Mahmoud, Environmental Science: Nano, 2018, 5, 1002-1011.
52. K. Wang, X. Zheng, M. Qi, W. Zhang, J. Du, Q. Han, C. Li, B. Dong, L. Wang and L. Xu, Sensors and Actuators B: Chemical, 2023, 390, 133955.
53. Y. Zhou, M. Li, H. Zheng, B. Huang and G. Liu, Journal of Materials Chemistry B, 2025, 13, 10225-10238.
54. E. Asadpour, H. R. Sadeghnia, A. Ghorbani, M. Sedaghat and M. T. Boroushaki, Journal of Nanoparticle Research, 2016, 18, 14.
55. A. Alshalani, N. AlAhmari, H. A. Amin, A. Aljedai and H. AlSudais, J Clin Med, 2025, 14.

View Article Online
DOI: 10.1039/D6TB00505E

56. F. Khodagholi, N. Ansari, M. Amini and S. K. Tusi, Cell Stress and Chaperones, 2012, 17, 409-422.
57. A. Weir, P. Westerhoff, L. Fabricius, K. Hristovski and N. Von Goetz, Environmental science & technology, 2012, 46, 2242-2250.
58. M. Duvvuri, S. Konkar, K. H. Hong, B. S. Blagg and J. P. Krise, ACS Chemical Biology, 2006, 1, 309-315.
59. E. Afjeh-Dana, P. Naserzadeh, H. Nazari, F. Mottaghitalab, R. Shabani, N. Aminii, B. Mehravi, F. T. Rostami, M. T. Joghataei and K. Mousavizadeh, International Journal of Biological Macromolecules, 2019, 129, 1034-1039.
60. H. Ahmadi, Z. Nayeri, Z. Minuchehr, F. Sabouni and M. Mohammadi, PloS one, 2020, 15, e0233088.
61. F. Shaki, M.-J. Hosseini, M. Ghazi-Khansari and J. Pourahmad, Biochimica et Biophysica Acta (BBA)-General Subjects, 2012, 1820, 1940-1950.
62. F. Dong, C. Fang, X. Yang, X. Zhang, F. Lopez and J. Ren, Diabetologia, 2006, 49, 1421-1433.
63. C. Sadegh and R. P. Schreck, Murj, 2003, 8, 39-43.
64. J. A. D. De Leon and C. R. Borges, Journal of visualized experiments: JoVE, 2020, 10.3791/61122.
65. P. Saeedi, I. Petersohn, P. Salpea, B. Malanda, S. Karuranga, N. Unwin, S. Colagiuri, L. Guariguata, A. A. Motala and K. Ogurtsova, Diabetes research and clinical practice, 2019, 157, 107843.
66. T. Meldgaard, S. S. Olesen, A. D. Farmer, K. Krogh, A. A. Wendel, B. Brock, A. M. Drewes and C. Brock, Journal of diabetes research, 2018, 2018, 3827301.
67. J. J. Yoo, D. W. Kim, M. Y. Kim, Y. T. Kim and J. H. Yoon, Journal of periodontology, 2019, 90, 576-583.
68. S.-Y. Yu, S.-K. Lee, B. Yang, H. Lee, H. J. Jeon and D.-H. Lee, J Korean Med Sci, 2024, 39.
69. B. Rohani, World journal of diabetes, 2019, 10, 485.
70. R. Ahmad and M. Haque, Diabetes, Metabolic Syndrome and Obesity, 2021, 3001-3015.
71. M. A. Nazir, L. AlGhamdi, M. AlKadi, N. AlBeajan, L. AlRashoudi and M. AlHussan, Open access Macedonian journal of medical sciences, 2018, 6, 1545.
72. M. Cui, J. Zhang, P. Han, L. Shi, X. Li, Z. Zhang, H. Bao, Y. Ma, Z. Tao and X. Dong, Materials Today Bio, 2024, 28, 101186.
73. M. Namvari, C. S. Biswas, M. Galluzzi, Q. Wang, B. Du and F. J. Stadler, Scientific Reports, 2017, 7.
74. J. Zhang, Y. Fu and A. Mo, International journal of nanomedicine, 2019, 10091-10103.
75. J. Li, Z. Li, X. Liu, C. Li, Y. Zheng, K. W. K. Yeung, Z. Cui, Y. Liang, S. Zhu and W. Hu, Nature Communications, 2021, 12, 1224.
76. F. Seidi, A. Arabi Shamsabadi, M. Dadashi Firouzjaei, M. Elliott, M. R. Saeb, Y. Huang, C. Li, H. Xiao and B. Anasori, Small, 2023, 19, 2206716.
77. E. A. Hussein, M. M. Zagho, B. R. Rizeq, N. N. Younes, G. Pintus, K. A. Mahmoud, G. K. Nasrallah and A. A. Elzatahry, International journal of nanomedicine, 2019, 4529-4539.
78. A. Rozmysłowska-Wojciechowska, J. Mitrzak, A. Szuplewska, M. Chudy, J. Woźniak, M. Petrus, T. Wojciechowski, A. S. Vasilchenko and A. M. Jastrzębska, Materials, 2020, 13, 2347.
79. D. Wang, L. Wang, Z. Lou, Y. Zheng, K. Wang, L. Zhao, W. Han, K. Jiang and G. Shen, Nano Energy, 2020, 78, 105252.
80. R. Song, L. Ren, H. Ma, R. Hu, H. Gao, L. Wang, X. Chen, Z. Zhao and J. Liu, American journal of translational research, 2016, 8, 4682.
81. G. F. Pierce, The American journal of pathology, 2001, 159, 399.
82. B. K. Tiwari, K. B. Pandey, A. Abidi and S. I. Rizvi, Journal of biomarkers, 2013, 2013, 378790.
83. M. Zhao, J. Zhou, L. YUAN, X.-q. ZHANG, Y. HU and H. YU, Journal of nutritional science and vitaminology, 2018, 64, 26-33.

View Article Online
DOI: 10.1039/D6TB00505E

84. X. Saelens, N. Festjens, L. V. Walle, M. v. Gurp, G. v. Loo and P. Vandenabeele, Oncogene, 2004, 23, 2861-2874.
85. F. Dong, C. X. Fang, X. Yang, X. Zhang, F. L. Lopez and J. Ren, Diabetologia, 2006, 49, 1421-1433.
86. A. D. Schimmer, Cancer research, 2004, 64, 7183-7190.
87. D. A. Breustedt, D. L. Schönfeld and A. Skerra, Biochimica et Biophysica Acta (BBA) - Proteins and Proteomics, 2006, 1764, 161-173.
88. A. Johnson, M. Francis and L. A. DiPietro, Advances in wound care, 2014, 3, 751-761.

View Article Online
DOI: 10.1039/D6TB00505E

Data availability statement

The authors declare that the data supporting the findings of this study are available within the paper and its Supplementary Information file.